# Supplemental material for "Direct determination of supermassive black hole properties with gravitational-wave radiation from surrounding stellar-mass black hole binaries"

## I. EXPLICIT EXPRESSIONS FOR VARIOUS TIMESCALES

Here we provide explicit expressions of various relevant timescales.

The instantaneous GW decay timescale is

$$\begin{aligned}\tau_{\rm gw} &= \frac{a}{|\dot{a}|} = \frac{5}{64}\frac{a^4}{\mu M_{\rm t}^2}\left[\frac{\left(1-e^2\right)^{7/2}}{1+\frac{73}{24}e^2+\frac{37}{96}e^4}\right], \\ &= 20\,{\rm yr}\left[\frac{\left(1-e^2\right)^{7/2}}{1+\frac{73}{24}e^2+\frac{37}{96}e^4}\right]\left(\frac{\mathcal{M}}{44\,M_\odot}\right)^{-5/3}\left(\frac{2f_{\rm orb}}{12\,{\rm mHz}}\right)^{-8/3},\end{aligned} \tag{1}$$

where $\mu$, $M_{\rm t}$, and $\mathcal{M}$ are respectively the reduced mass, total mass, and the chirp mass of the binary of interest. In the second line we have scaled the number by the orbital frequency for future convenience, though we remind the reader that the timescale defined here is the instantaneous decay rate of the semi-major axis (instead of frequency). Furthermore, when the orbit is circular, the GW radiation has a single frequency component with $f = 2f_{\rm orb}$, and thus a factor of 2 is included in the scaling of $f_{\rm orb}$.

For a circular orbit, the total time to merger is $t_{\rm m} = \tau_{\rm gw}/4$. By setting $t_{\rm m} = T_{\rm obs} = 5\,{\rm yr}$ (the fiducial observation time), we can then determine the initial frequency (or the initial orbital separation) for a given binary system. This is why we chose an initial GW frequency $f^{(0)} = 2f_{\rm orb} = 12\,{\rm mHz}$ ($a_{\rm i}^{(0)} = 1.4\times10^{-3}\,{\rm AU}$) for the binary with $M_1 = M_2 = 50\,M_\odot$ and $f^{(0)} = 2f_{\rm orb} = 4.4\,{\rm mHz}$ ($a_{\rm i}^{(0)} = 4.7\times10^{-3}$) for the one with $M_1 = M_2 = 250\,M_\odot$ (see Fig. 3 in the main text). In comparison, for a typical outer orbit with $M_1 + M_2 = 100\,M_\odot$, $M_3 = 10^8\,M_\odot$, and $a_{\rm o} = 100M_3 \simeq 100\,{\rm AU}$, the merger time is $t_{\rm m,o} \simeq 3\times10^7\,{\rm yr}$. Therefore, in most cases we can safely ignore the GW-induced decay of the outer orbit.

The presence of the central SMBH will modulate the GW waveform emitted by the inner binary (i.e., the carrier) via various effects. The most significant one is the Doppler phase shift due to the motion of the outer orbit (Newtonian dipole effect), at a rate $\Omega_{\rm o} \simeq \sqrt{M_3/a_{\rm o}^3}$, or a period

$$P_{\rm o} = \frac{2\pi}{\Omega_{\rm o}} = 0.1\,{\rm yr}\left(\frac{M_3}{10^8\,M_\odot}\right)\left(\frac{a_{\rm o}}{100M_3}\right)^{3/2}. \tag{2}$$

The next leading-order effect is the de Sitter-like precession of the inner orbit (a 1.5 post-Newtonian-order, or 1.5 PN effect), which is the focus of the main text. It has a rate [1, 2]

$$\Omega_{\rm dS} = \frac{3}{2}\frac{M_3+\mu_{\rm o}/3}{a_{\rm o}(1-e_{\rm o}^2)}\Omega_{\rm o} \simeq \frac{3}{2}\frac{M_3}{a_{\rm o}(1-e_{\rm o}^2)}\Omega_{\rm o}, \tag{3}$$

where the second equality applies because $M_3 \gg \mu_{\rm o} \simeq (M_1+M_2)$. The corresponding period is thus

$$P_{\rm dS} = 6.5\,{\rm yr}\left(1-e_{\rm o}^2\right)\left(\frac{M_3}{10^8\,M_\odot}\right)\left(\frac{a_{\rm o}}{100M_3}\right)^{5/2}. \tag{4}$$

When the central SMBH is fast spinning, the inner orbit will also precess around the spin of the SMBH $\boldsymbol{S}_3$ by the Lense-Thirring effect (2 PN). Its rate is

$$\Omega_{\rm LT} = \frac{S_3}{a_{\rm o}^3(1-e_{\rm o})^{3/2}}, \tag{5}$$

and period

$$P_{\rm LT} = 2.0\times10^2\,{\rm yr}(1-e_{\rm o}^2)^{3/2}\left(\frac{S_3}{M_3^2}\right)\left(\frac{M_3}{10^8\,M_\odot}\right)\left(\frac{a_{\rm o}}{100M_3}\right)^3. \tag{6}$$

Additionally, the SMBH may perturb the inner orbit via the Lidov-Kozai effect (i.e., the Newtonian tidal effect as it comes at the quadrupole order). The rate is given by [1]

$$\Omega_{\rm LK} = \frac{M_3}{(M_1+M_2)}\left(\frac{a_{\rm i}}{a_{\rm o}\sqrt{1-e_{\rm o}^2}}\right)^3 \Omega_i, \tag{7}$$

where $\Omega_{\rm i} = \sqrt{(M_1+M_2)/a_{\rm i}^3}$ is the orbital frequency of the inner orbit. The corresponding period is thus

$$P_{\rm LK} = 1.8\times10^3\,{\rm yr}(1-e_{\rm o}^2)^{3/2}\left(\frac{M_3}{10^8\,M_\odot}\right)^2\left(\frac{a_{\rm o}}{100M_3}\right)^3\left(\frac{M_1+M_2}{100\,M_\odot}\right)^{1/2}\left(\frac{a_{\rm i}}{1.4\times10^{-3}\,{\rm AU}}\right)^{-3/2}. \tag{8}$$

Unlike the de Sitter and Lense-Thirring effects which are independent of $a_{\rm i}$, the Lidov-Kozai timescale increases as the inner orbit decays because the "lever arm" for the SMBH to perturb is smaller. The Lidov-Kozai effect is therefore less and less significant as the inner binary evolves towards the merger.

As the inner binary may reside in a gaseous disk, the frictional force from the background gas may both cause the inner binary as a whole to accelerate/decelerate from the Keplerain outer orbit, and harden the inner binary and make it merges in a shorter timescale than $t_{\rm m}$.

For the gaseous effect on the outer orbit, we estimate it with the dynamical friction derived in Ref. [3], which leads to a characteristic timescale [4]

$$\tau_{\rm gas} \equiv \frac{a_{\rm o}}{|\dot{a}_{\rm o,gas}|} = 8\times10^5\,{\rm yr}\left(\frac{\rho_{\rm bg}}{10^{-8}\,{\rm g\,cm^{-3}}}\right)^{-1}\left(\frac{M_1+M_2}{100\,M_\odot}\right)^{-1}\left(\frac{a_{\rm o}}{100M_3}\right)^{-3/2}, \tag{9}$$

where $\dot{a}_{\rm o,gas}$ is the rate at which the outer orbit changes due to the hydrodynamic drag and $\rho_{\rm bg}$ is the background gas density. Although this effect may be important for the migration of the outer orbit over the entire evolution of the inner binary, over a period of $T_{\rm obs}\simeq 5\,{\rm yr}$, it only changes the outer orbit by a fractional amount of $T_{\rm obs}/\tau_{\rm gas}\sim10^{-5}$ and can thus be safely ignored.

As for the inner binary, a circumbinary mini-accretion disk may form. In this scenario, the inner binary hardens due to the gaseous effect over a timescale [4]

$$\tau'_{\rm gas} = 4\times10^3\,{\rm yr}\times q^{-1}\left(\frac{2}{1+q}\right)^{-3}\left(\frac{M_1}{50\,{\rm M}_\odot}\right)^{-1}\left(\frac{\rho_{\rm bg}}{10^{-13}\,{\rm g\,cm^{-3}}}\right)^{-1}\left(\frac{c_{\rm s}}{10^2\,{\rm km\,s^{-1}}}\right)^3, \tag{10}$$

where $q=M_2/M_1$. A similar estimation can be found in Ref. [5] where the authors found the inspiraling rate changes from gas dominated to GW dominated at an inner separation of $a_{\rm i}\sim R_\odot\simeq 5\times10^{-3}\,{\rm AU}$. For the typical $a_{\rm i}$ we consider, this then indicates $\tau'_{\rm gas}\sim100\tau_{\rm gw}$.

Ref. [6] suggested yet another hardening mechanism due to the formation of overdense spiral tails lagging the BHs in the inner binary and exerting torques on them. This mechanism could efficiently half the inner semi-major axis in a few cycles of the outer orbit, and for $a_{\rm o}\sim100M_3$, such a timescale could be comparable to the duration of observation. Nonetheless, the model considered by Ref. [6] applies for inner binaries with separations of $a_{\rm i}\sim r_{\rm H}$, where $r_{\rm H}=a_{\rm o}\,[M_3/3(M_1+M_2)]^{1/3}$ is the Hill radius. For $a_{\rm o}=100\,M_3$ and $M_3=10^8\,M_\odot$ ($M_3=10^6\,M_\odot$), we have $r_{\rm H}\simeq0.7\,{\rm AU}$ ($r_{\rm H}\simeq0.03\,{\rm AU}$), much greater than the initial inner binary's separation of $a_{\rm i}\simeq1.4\times10^{-3}\,{\rm AU}$ considered in our work. Therefore, our case is likely to be beyond the regime of validity of the model proposed in [6] (see also the discussion in sec. 8.5 of Ref. [6] and sec. 2.3 of Ref. [7]). As a result, this is an effect critical for the early evolution of the inner binary but is likely subdominant for the final state when $\tau_{\rm gw}=\mathcal{O}(10\,{\rm yr})$.

Furthermore, as shown in Ref. [4], the gaseous friction's effect on the inner binary is make the chirp mass appear heavier than the true value by a factor $(1+\tau'_{\rm gas}/\tau_{\rm gw})^{3/5}$. It can therefore be absorbed into the carrier waveform $\tilde{h}_{\rm c}$ and be extracted from the frequency evolution of the waveform similar to high-order post-Newtonian parameter.

The inner binary, after formation, may also experience multiple encounter with the surrounding background stars/BHs. The typical timescale between two consecutive interactions can be estimated to be [8, 9]

$$\tau_{\rm enc} = 2\times10^5\,{\rm yr}\left(\frac{\sigma}{0.01}\right)\left(\frac{n_{\rm bg}}{10^{10}\,{\rm pc^{-3}}}\right)\left(\frac{r_{\rm p}}{0.01\,{\rm AU}}\right)^{-1}\left(\frac{M_1+M_2}{100\,M_\odot}\right)^{-1}\left(\frac{M_{\rm bg}}{10\,M_\odot}\right)^{-1/2}, \tag{11}$$

where $\sigma$ is the velocity dispersion, $n_{\rm bg}$ the number density of background stars/BHs, $r_{\rm p}$ the maximum considered close approach to the inner binary, and $M_{\rm bg}$ the mass of the background perturber. In the scaling above, we have conservatively (making $\tau_{\rm enc}$ smaller) set $\sigma=0.1v_{\rm orb}(a_{\rm o}=100\,M_3)$ and $r_{\rm p}\simeq10a_{\rm i}$. Note $\tau_{\rm enc}\propto r_{\rm p}^{-1}\sim a_{\rm i}^{-1}$, and

therefore encounters with background objects are important when the inner binary is far apart (e.g., when it is just formed). The frequent encounters at the early stages also play a critical role in giving the inner binary a nearly isotropic orientation so that $\boldsymbol{L}_{\rm i}$ is typically misaligned with $\boldsymbol{L}_{\rm o}$. However, at the end stage of the inner binary's evolution with $\tau_{\rm gw} \sim T_{\rm obs}$, we have $\tau_{\rm gw} \ll \tau_{\rm enc}$, and therefore it is very unlikely for the inner binary to be disrupted during the observation.

## II. EXPLICIT EXPRESSIONS FOR THE WAVEFORMS

Here we provide explicit expressions for various quantities used in our construction of the waveform.

The "carrier" waveform in our study is given by

$$\tilde{h}_{\rm C}(f) = \left(\frac{5}{96}\right)^{1/2} \frac{\mathcal{M}^{5/6}}{\pi^{2/3} D_L} f^{-7/6} \exp\left\{ {\rm i} \left[ 2\pi f t_{\rm c} - \phi_{\rm c} - \frac{\pi}{4} + \frac{3}{4}(8\pi\mathcal{M}f)^{-5/3} \right] \right\}. \tag{12}$$

The antenna pattern coefficients are

$$F_+(\theta_{\rm S}, \phi_{\rm S}, \psi_{\rm S}) = \frac{1}{2}\left(1+\cos^2\theta_{\rm S}\right)\cos 2\phi_{\rm S}\cos 2\psi_{\rm S} - \cos\theta_{\rm S}\sin 2\phi_{\rm S}\sin 2\psi_{\rm S}, \tag{13}$$

$$F_\times(\theta_{\rm S}, \phi_{\rm S}, \psi_{\rm S}) = \frac{1}{2}\left(1+\cos^2\theta_{\rm S}\right)\cos 2\phi_{\rm S}\sin 2\psi_{\rm S} + \cos\theta_{\rm S}\sin 2\phi_{\rm S}\cos 2\psi_{\rm S}, \tag{14}$$

where $(\theta_{\rm S}, \phi_{\rm S})$ are the polar coordinates of $\hat{\boldsymbol{N}}$ in the time-varying $(x, y, z)$ frame, and

$$\psi_{\rm S} = \tan^{-1}\left[ \hat{\boldsymbol{L}}_{\rm i} \cdot \hat{\boldsymbol{z}} - \frac{(\hat{\boldsymbol{L}}_{\rm i}\cdot\hat{\boldsymbol{N}})(\hat{\boldsymbol{z}}\cdot\hat{\boldsymbol{N}})}{\hat{\boldsymbol{N}}\cdot(\hat{\boldsymbol{L}}_{\rm i}\times\hat{\boldsymbol{z}})} \right] \tag{15}$$

is the polarization angle of the source.

We calculate the Thomas phase $\Phi_{\rm T}$ by integrating

$$\Phi_{\rm T}(t) = -\int_t^{t_{\rm c}} dt \left[ \frac{\hat{\boldsymbol{L}}\cdot\hat{\boldsymbol{N}}}{1-\left(\hat{\boldsymbol{L}}\cdot\hat{\boldsymbol{N}}\right)^2} \right] \left(\hat{\boldsymbol{L}}\times\hat{\boldsymbol{N}}\right)\cdot\frac{d\hat{\boldsymbol{L}}}{dt}, \tag{16}$$

and the polarization phase $\Phi_{\rm P}$ from the relation

$$\Phi_{\rm P}(t) = \arctan\left[ \frac{-A_\times(t)F_\times(t)}{A_+(t)F_+(t)} \right]. \tag{17}$$

The time-dependent orientation of $\hat{\boldsymbol{L}}_{\rm i}$ in our case is given by

$$\begin{aligned} \hat{\boldsymbol{L}}_{\rm i} = & \left[\cos\lambda_L \sin\overline{\theta}_J \cos\overline{\phi}_J + \sin\lambda_L \left(-\cos\overline{\theta}_J\cos\overline{\phi}_J\cos\alpha + \sin\overline{\phi}_J\sin\alpha\right)\right]\hat{\bar{\boldsymbol{x}}} \\ & + \left[\cos\lambda_L \sin\overline{\theta}_J \sin\overline{\phi}_J - \sin\lambda_L \left(\cos\overline{\phi}_J\sin\alpha + \cos\overline{\theta}_J\sin\overline{\phi}_J\cos\alpha\right)\right]\hat{\bar{\boldsymbol{y}}} \\ & + \left[\cos\lambda_L\cos\overline{\theta}_J + \sin\lambda_L\sin\overline{\theta}_J\cos\alpha\right]\hat{\bar{\boldsymbol{z}}}, \end{aligned} \tag{18}$$

where $\alpha = \Omega_{\rm dS} t + \alpha_0$.

The detector's orientations are

$$\hat{\boldsymbol{z}}(t) = -\frac{\sqrt{3}}{2}\left(\cos\phi_{\rm d}\hat{\bar{\boldsymbol{x}}} + \sin\phi_{\rm d}\hat{\bar{\boldsymbol{y}}}\right) + \frac{1}{2}\hat{\bar{\boldsymbol{z}}}. \tag{19}$$

$$\hat{\boldsymbol{x}}(t) = -\frac{\sin 2\phi_{\rm d}}{4}\hat{\bar{\boldsymbol{x}}} + \frac{3+\cos 2\phi_{\rm d}}{4}\hat{\bar{\boldsymbol{y}}} + \frac{\sqrt{3}}{2}\sin\phi_{\rm d}\hat{\bar{\boldsymbol{z}}} \tag{20}$$

and $\hat{\boldsymbol{y}} = \hat{\boldsymbol{z}}\times\hat{\boldsymbol{x}}$. In the expressions above, $\phi_{\rm d} = 2\pi t/{\rm yr}$ is the phase of the detector.

To summarize, when we consider the simple-precession problem, the waveform is parameterized in terms 11 free parameters in total, $(\mathcal{M}, D_{\rm L}, t_{\rm c}, \phi_c, \overline{\theta}_{\rm S}, \overline{\phi}_{\rm S}, \overline{\theta}_J, \overline{\phi}_J, P_{\rm dS}, \lambda_L, \alpha_0)$. When consider the full SMBH effects (dS precession and Doppler shift due to the outer orbital motion), we further write $P_{\rm dS}$ in terms of $M_3$ and $a_{\rm o}$, and include $\phi^{(0)}$ as the initial phase of the outer orbit's Doppler phase.

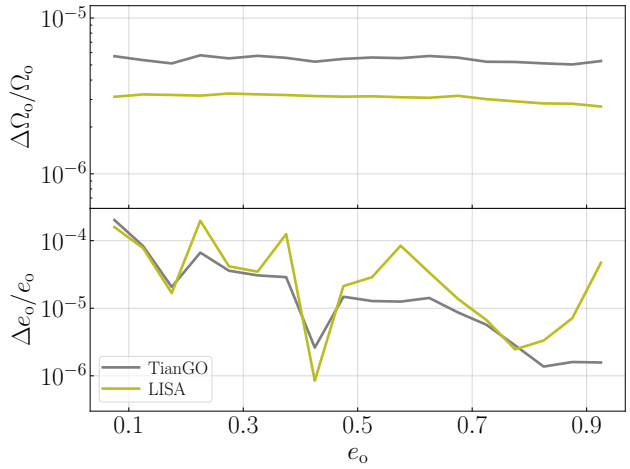


FIG. 1. Fractional uncertainties in $\Omega_o$ (top) and $e_o$ (bottom) as a function of $e_o$. The grey (olive) trace assumes the sensitivity of TianGO (LISA). We have dropped other antenna responses and used the angle-averaged sensitivity when evaluating the Fisher matrix ($\sqrt{5}$ times greater than the intrinsic noise). When generating the waveform, we have used $2\pi/\omega_o = 0.51\,\mathrm{yr}$ and $\mathcal{A} = 212\,\mathrm{AU}$, which can be further realized with $M_3 = 10^8\,M_\odot$, $a_o = 300M_3$, and $\iota = 45^\circ$.

## III. DOPPLER PHASE SHIFT OF ELLIPTIC OUTER ORBITS

Here we demonstrate that we can extract simultaneously the orbital period (hence the enclosed mass density) and eccentricity of an elliptic outer orbit from the Doppler phase shift alone.

To do so, we consider a simple model with $\tilde{h}(f) = \tilde{h}_C(f)\exp[-i\Phi_D(t)]$. In other words, we include only the Doppler phase shift due to the outer orbit (now has finite eccentricity) and drop other antenna responses for simplicity. The Doppler phase can be further written as

$$\Phi_D(t) = 2\pi f r_{o,\parallel}(t), \tag{21}$$

where $r_{o,\parallel}(t)$ is the orbital separation projected along the line of sight. Specifically, we have

$$r_{o,\parallel}(t) = \frac{\mathcal{A}(1-e_o^2)}{1+e_o\cos u(t)}\sin[u(t)+\gamma], \tag{22}$$

where $u(t)$ and $\gamma$ are the true anomoly and the argument of pericenter.[10] The amplitude is further given by $\mathcal{A} = a_o\sin\iota$. Note that with Doppler shift alone we cannot separate out $a_o$ and $\sin\iota$, and thus we treat $\mathcal{A}$ itself as a free parameter. The true anomoly can be solved as a function of time (which is further a fucntion of the GW frequency of the inner orbit) via the differential equation

$$\dot{u} = \Omega_o\frac{(1+e_o\cos u)^2}{(1-e_o^2)^{3/2}}, \tag{23}$$

where $\Omega_o = \sqrt{M_3/a_o^3}$. In summary, the Doppler shift can be parameterized in terms of 5 parameters: $(\Omega_o, e_o, \mathcal{A}, \gamma, u_c)$ with $u_c = u(t = t_c)$, and our goal here is to illustrate that $\Omega_o$ and $e_o$ can both be measured with high accuracy.

In Figure 1 we demonstrate the detectability of $\Omega_o$ (top panel) and $e_o$ (bottom panel) as a function of $e_o$ using respectively the sky-averaged sensitivity [11] of TianGO (grey) and LISA (olive). To model the Doppler phase $\Phi_D$, we have further assumed $2\pi/\omega_o = 0.51\,\mathrm{yr}$ and $\mathcal{A} = 212\,\mathrm{AU}$. This set of parameters can be further realized by a physical system with $M_3 = 10^8\,M_\odot$, $a_o = 300M_3$, and $\iota = 45^\circ$. For reference, the de Sitter precession period for such a system would be $2\pi/\Omega_{dS} = 101\,\mathrm{yr}$ if $e_o = 0$ and $19\,\mathrm{yr}$ if $e_o = 0.9$. The values of $\gamma$ and $u_c$ are both randomized over when generating the plot. Consistent with the main text, we assumed $M_1 = M_2 = 50\,M_\odot$ and $D_L$ for the carrier (in fact, only the chirp mass $\mathcal{M} = 44\,M_\odot$ matters as we use the leading-order quadrupole formula for the carrier) and the initial frequency is set to $f^{(0)} = 12\,\mathrm{mHz}$ so that the system merges in $T_{obs} = 5\,\mathrm{yr}$.

As shown in the plot, the frequency $\Omega_o$ is essentially independent of the eccentricity of the outer orbit $e_o$ and it can be constrained to a high accuracy of $\Delta\Omega_o/\Omega_o \sim$ a few $\times\,10^{-6}$ by both TianGO and LISA. The fractional error in $e_o$ shows more scattering due to the randomness of $\gamma$ and $u_c$, yet there is a trend that the fractional error decreases as $e_o$ increases. Even in the worst cases, we still have $\Delta e_o/e_o \lesssim 10^{-4}$. We therefore conclude that both $\Omega_o$ and $e_o$

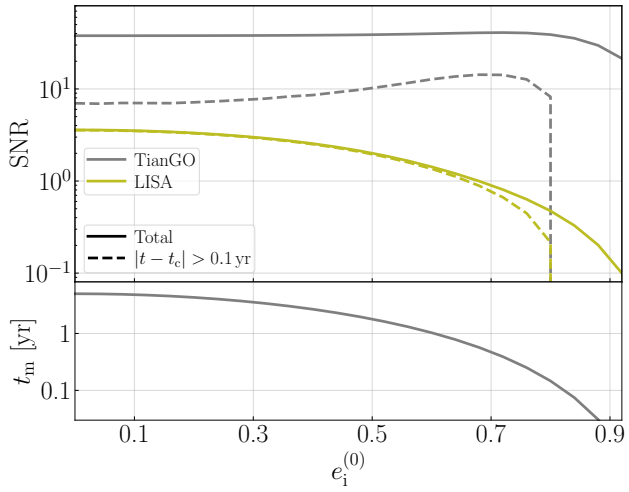


FIG. 2. Sky-averaged SNR and merger time as a function of the initial eccentricity of the inner orbit, $e_{\rm i}^{(0)}$. The solid trace is the total SNR using all the data and the dashed trace uses only data at least 0.1 yr prior to the merger so that this portion is accumulated over a time comparable to the typical precession period. We have fixed the initial semi-major axis of the inner binary to be $a_{\rm i}^{(0)} = 1.4 \times 10^{-3}\,\mathrm{AU}$ so that a circular binary can merge in 5 years. If the eccentricity is high ($> 0.7$), we would be able to observe the inner binary starting from a much greater $a_{\rm i}$ so that it still stays in band for years with an SNR of few during the early stage evolution (assuming TianGO's sensitivity; see the discussions in the text).

can indeed be well constrained from the Doppler phase even for elliptic outer orbits. Once we combine them with the period of the de Sitter precession $\Omega_{\rm dS} \simeq 3M_3\Omega_{\rm o}/\left[2a_{\rm o}(1-e_{\rm o}^2)\right]$ as discussed in the main text, we can therefore simultaneously determine both the mass of the center SMBH $M_3$ and the key properties of the outer orbit $(a_{\rm o}, e_{\rm o})$.

In fact, the de Sitter precession also allows us to infer the inclination angle of the outer orbit and thus $\sin\iota$. As a result, we can also infer $a_{\rm o}$ from the amplitude $\mathcal{A}$ which makes the parameter inference even more accurate. Similarly, the precession of the pericenter (i.e., $\gamma$) would also provide additional constraints on $(M_3, a_{\rm o}, e_{\rm o})$ and enhance the accuracy further.

## IV. SNR OF ELLIPTIC INNER ORBITS

We now turn to study the effects of the eccentricity of the inner orbit.

First, we note that the observed waveform can be modeled as the product $\tilde{h}(f) = \Lambda(f)\tilde{h}_{\rm C}(f)$ with $\Lambda$ the antenna response and $\tilde{h}_{\rm C}$ the antenna-independent waveform of the carrier. We can consequently call parameters that affects only $\Lambda$ the extrinsic parameters (including $M_3$, $a_{\rm o}$, $e_{\rm o}$, $\lambda$, etc.), and those affecting only $\tilde{h}_{\rm C}$ the intrinsic parameters (including $e_{\rm i}$).

If we ignore the covariance between different elements, the error of an extrinsic parameter $\Delta\theta^{(\rm ext)}$ scales as

$$\Delta\theta^{(\rm ext)} \sim \frac{1}{|\partial\tilde{h}/\partial\theta^{(\rm ext)}|} = \frac{1}{|\left[\partial\Lambda/\partial\theta^{(\rm ext)}\right]\tilde{h}_{\rm c}|}. \tag{24}$$

Therefore, we can see an intrinsic parameter such as $e_{\rm i}$ affects the detectability of an extrinsic one (such as $M_3$) mostly through changing the overall signal-to-noise-ratio (SNR). Consequently, we can estimate how the inner eccentricity affects the results we drawn in the main text based on circular orbits by considering its effects on the SNR.

To estimate the SNR of an elliptic inner orbit, we consider the characteristic strain of the system. Specifically, we can first decompose the time-domain waveform into a sum over harmonics as $h(t) = \sum_k h_k(t)$ with each harmonic oscillating at a frequency $f_k$. Up to corrections due to the precession of the inner pericenter, we have $f_k \simeq k f_{\rm i}$ with $2\pi f_{\rm i} = \sqrt{(M_1+M_2)/a_{\rm i}^3}$. The characteristic strain for each harmonic is thus given by

$$h_{{\rm c},k} = \frac{1}{\pi D_{\rm L}}\sqrt{\frac{2\dot{E}_k}{\dot{f}_k}}, \tag{25}$$

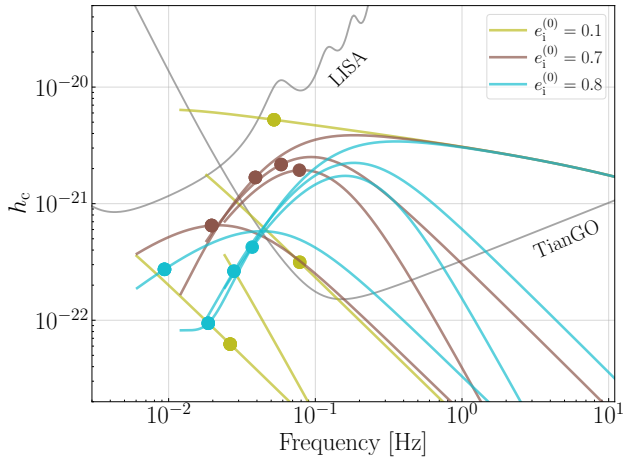


FIG. 3. Characteristic strain $h_c$ of the inner orbit for representative initial eccentricities $e_{\rm i}^{(0)}$ (represented by different colors). The initial semi-major axis is fixed to $a_{\rm i}^{(0)} = 1.4 \times 10^{-3}\,{\rm AU}$. For each configuration we only show the first 4 harmonics. The dot markers correspond to the instant when the inner binary is 0.1 yr prior to the final merger.

where $\dot{E}_k$ is the GW power radiated to infinity at $f_k$. The SNR can then be obtained by summing over harmonics as

$$\mathrm{SNR}^2 = \sum_k \int \frac{h_{{\rm c},k}^2(f_k)}{5 f_k S_{\rm n}(f_k)} d\ln f_k, \tag{26}$$

where $S_{\rm n}$ is the power-spectral density of the instrument noise. Here we drop the antenna response and use the sky-averaged sensitivity instead (which leads to the numerical factor of 5 in the denominator). We refer the interested readers to Ref. [12] for more details of the calculation.

One such example is shown in the top panel of Fig. 2. Here we consider an inner binary with masses of $M_1 = M_2 = 50\,M_\odot$ and an initial semi-major axis of $a_{\rm i}^{(0)} = 1.4 \times 10^{-3}\,{\rm AU}$ (same as the one considered in the main text). We vary the initial eccentricity $e_{\rm i}^{(0)}$ and compute the SNR based on the characteristic strains using both the sensitivity of TianGO (grey traces) and LISA (olive traces). In addition to the total SNR shown in the solid traces, we also consider the SNR using only the data at least 0.1 yr prior to the final merger (shown in the dashed traces). This portion of the data is accumulated over a time comparable to the typical de Sitter precession periods of a few to tens of years and would thus directly helps constraining the time-varying antenna pattern. For reference, we also show the total time to merger $t_{\rm m}$ in the bottom panel.

As shown in the plot, if the inner binary's eccentricity is mild ($e_{\rm i}^{(0)} \lesssim 0.7$; this corresponds to about half of the sources if $e_{\rm i}^{(0)}$ yields a thermal distribution), then both TianGO and LISA see mild changes in both the total SNR and that accumulated from the early stage only. In fact, the SNR seen by TianGO increases slightly first with an increasing eccentricity. This can be understood by examining Fig. 3. As the eccentricity increases, more GW power are emitted through high-order harmonics (instead of through only the $k = 2$ harmonic for circular orbits). These harmonics have higher frequencies and therefore are in the band where a decihertz detector like TianGO is more sensitive. For LISA, the SNR is reduced by a factor of 3 but is still above unity as $e_{\rm i}^{(0)}$ changes from 0 to 0.7. These should not change our results qualitatively.

When the initial eccentricity is more extreme, $e_{\rm i}^{(0)} \gtrsim 0.8$, the inner binary would merge within 0.1 yr and therefore the dashed line vanishes. However, this is an artifact of our fixing $a_{\rm i}^{(0)} = 1.4 \times 10^{-3}\,{\rm AU}$, a value chosen so that our inner binaries (with circular orbits) would merge within 5 years, the fiducial duration of observation $T_{\rm obs}$. In fact, once we allow the inner orbit to be eccentric, we can in fact capture the binary when it is at a much greater orbital separation. For example, an inner binary with $(a_{\rm i}, 1 - e_{\rm i}) = (1.4 \times 10^{-3}\,{\rm AU}, 0.2)$ can be further evolved from $(a_{\rm i}, 1 - e_{\rm i}) = (0.05\,{\rm AU}, 6 \times 10^{-3})$ [note that as shown in Ref. [2], $(1 - e) \propto a^{-1}$ when $(1 - e) \ll 1$; also note that the Newtonian tide could be important for such an highly eccentric binary with a large semi-major axis, especially if $M_3 \lesssim 10^7\,M_\odot$] in slightly less than 2 years $< T_{\rm obs}$. During this process, the $k \simeq 3,000$ to $k \simeq 300$ harmonics consecutively sweep through TianGO's most sensitive band, and together they contribute an SNR of 5.3 over the 2-year evolution. As a result, even for significantly eccentric inner binaries, it is still possible to obtain an SNR of a few with an integration time over a year to constrain the time-varying antenna pattern induced by the central SMBH.

[1] B. Liu, D. Lai, and Y.-H. Wang, Binary Mergers near a Supermassive Black Hole: Relativistic Effects in Triples, ApJ **883**, L7 (2019), arXiv:1906.07726 [astro-ph.HE].

[2] H. Yu, S. Ma, M. Giesler, and Y. Chen, Spin and eccentricity evolution in triple systems: From the Lidov-Kozai interaction to the final merger of the inner binary, Phys. Rev. D **102**, 123009 (2020), arXiv:2007.12978 [gr-qc].

[3] E. C. Ostriker, Dynamical Friction in a Gaseous Medium, ApJ **513**, 252 (1999), arXiv:astro-ph/9810324 [astro-ph].

[4] X. Chen, Z.-Y. Xuan, and P. Peng, Fake Massive Black Holes in the Milli-Hertz Gravitational-wave Band, ApJ **896**, 171 (2020), arXiv:2003.08639 [astro-ph.HE].

[5] A. Antoni, M. MacLeod, and E. Ramirez-Ruiz, The Evolution of Binaries in a Gaseous Medium: Three-dimensional Simulations of Binary Bondi-Hoyle-Lyttleton Accretion, ApJ **884**, 22 (2019), arXiv:1901.07572 [astro-ph.HE].

[6] C. Baruteau, J. Cuadra, and D. N. C. Lin, Binaries Migrating in a Gaseous Disk: Where are the Galactic Center Binaries?, ApJ **726**, 28 (2011), arXiv:1011.0360 [astro-ph.GA].

[7] I. Bartos, B. Kocsis, Z. Haiman, and S. Márka, Rapid and Bright Stellar-mass Binary Black Hole Mergers in Active Galactic Nuclei, ApJ **835**, 165 (2017), arXiv:1602.03831 [astro-ph.HE].

[8] K. Gültekin, M. C. Miller, and D. P. Hamilton, Growth of Intermediate-Mass Black Holes in Globular Clusters, ApJ **616**, 221 (2004), arXiv:astro-ph/0402532 [astro-ph].

[9] F. Antonini and F. A. Rasio, Merging Black Hole Binaries in Galactic Nuclei: Implications for Advanced-LIGO Detections, ApJ **831**, 187 (2016), arXiv:1606.04889 [astro-ph.HE].

[10] Here we treat $\gamma$ as a constant for simplicity and ignore the general-relativistic precession of the pericenter which happens at a rate $\Omega_e \simeq 3M_3\Omega_{\rm o}/\left[a_{\rm o}(1-e_{\rm o}^2)\right] \simeq 2\Omega_{\rm dS}$. Including it would introduce more dynamics on the system without needing extra unknown parameters. Consequently it would make the constraints on $(M_3, a_{\rm o}, e_{\rm o})$ even better.

[11] É. É. Flanagan and S. A. Hughes, Measuring gravitational waves from binary black hole coalescences. I. Signal to noise for inspiral, merger, and ringdown, Phys. Rev. D **57**, 4535 (1998), arXiv:gr-qc/9701039 [gr-qc].

[12] L. Barack and C. Cutler, LISA capture sources: Approximate waveforms, signal-to-noise ratios, and parameter estimation accuracy, Phys. Rev. D **69**, 082005 (2004), arXiv:gr-qc/0310125 [gr-qc].